ELSEVIER

Journal of Nuclear Materials 241–243 (1997) 92–104

journal of nuclear materials

Radiative edge layers in limiter tokamaks

P. Monier-Garbet *

Association Euratom-CEA sur la fusion, Département de recherches sur la fusion contrôlée, Centre d'études de Cadarache, F-13108 Saint-Paul-lez-Durance, France

Abstract

The characteristics of the highly radiative edge layers produced in the limiter configuration and with an open ergodic divertor are reviewed, with emphasis on the results obtained in TEXTOR and Tore Supra. In these two experiments an impurity injection technique is used to obtain highly radiating homogeneous peripheral layers. This requires that the peripheral radiation capability be maximized, while at the same time avoiding plasma core contamination; it is also necessary to insure the stability of the radiating layer. These physics issues, governing the success of the highly radiative edge scenario, are discussed.

Keywords: Tore Supra; TEXTOR; Boundary plasma; Impurity transport; Radiation asymmetry

1. Introduction

Energy and particle exhaust is one of the crucial issues for the success of the next generation of high fusion power tokamaks such as ITER. If all of the heating power in ITER strikes the divertor plates, the peak heat flux on the plasma facing components will be in the range of 20 to 40 MW/m^2. Such heat loads are far too high for stationary operation. For a safe divertor design, it is generally admitted that the peak heat loads should be in the range of 0.6–4 MW/m^2 [1]. A large reduction of the peak heat loads on the divertor plates can be achieved if a large fraction of the heating power can be radiated either in the divertor volume ('radiative divertor'), or in the main plasma edge ('radiative edge layer' or 'radiative mantle'). During the past few years, the radiative divertor scenarios have been tested in most axisymmetric poloidal divertor tokamaks [2–4]. In this paper, the concept involving significant radiation losses from the main plasma edge is addressed. For this scenario, the high radiative loss is triggered either by deuterium or gaseous impurity injection. Therefore the main difficulties lie, firstly, in minimizing the plasma core contamination by the injected species, and secondly, in maintaining the thermal and MHD stability of the edge layer. High radiation level in the edge, low contamination of the plasma core, stability of the radiating boundary are the three major requirements for achieving the success of the radiative mantle scenario. These three requirements have been fulfilled in the TEXTOR experiments where a stationary high level of edge radiation has been obtained by using silicon and/or neon as radiating impurities [5]. In Tore Supra, stable operation has been demonstrated using neon injection, both in the limiter and ergodic divertor (ED) configurations [6,7]. The goal of this paper is to discuss and compare the global characteristics of the edge radiative layers that have been produced in different tokamaks, with emphasis on the results obtained in TEXTOR and Tore Supra.

TEXTOR is a medium-size tokamak with a circular plasma having a major radius $R = 1.75$ m and a minor radius $a = 0.46$ m. The standard values are $B_t = 2.25$ T for the toroidal magnetic field and $I_p = 350$ kA for the plasma current. The toroidal belt limiter ALT-II is used as a pump limiter. All limiter blades are made of graphite and the

* Tel.: +33-4 42 25 61 37; fax: +33-4 42 25 62 33; e-mail: monier@drfc.cad.cea.fr.

PII S0022-3115(96)00498-9

vessel wall is either boronized or siliconized. The working gas is deuterium or hydrogen. Auxiliary heating with neutral beam (NBI) co- or counter-injection (1.4 MW each) and ion-cyclotron resonance heating (ICRH, 2 MW) are available. The standard condition in this paper is the NBI co-injection case in combination with ICRH, so that together with ohmic heating (0.3 MW) a total heating power up to ≈ 3.7 MW could be applied. This corresponds to an average power density of ≈ 0.5 MW/m^3 and a radial power flow to the edge of ≈ 0.11 MW/m^2, which is relevant for ITER. Injection of gaseous impurities like neon or silicon containing compounds (silane and di-silane) is achieved via a gas puffing system with a fast piezoelectric valve. Radiated fractions ($\gamma = P_{rad}/P_{tot}$) up to 0.9 have been obtained in stationary conditions [8]. This corresponds to a maximum radiated power of $P_{rad} \approx 3.5$ MW.

Similar experiments have been performed in Tore Supra, a circular cross-section limiter tokamak, equipped with a set of ergodic divertor coils. Therefore, Tore Supra gives the possibility to compare the production of radiative layers in limiter and divertor configurations. In the ED configuration, the magnetic surfaces in the plasma edge are destroyed with a weak resonant perturbation [9], thus leading to an edge layer where the field lines are stochastic. In fact, the most extended zone (the so-called laminar zone [10]) consists essentially of an extended scape-off-layer (SOL), where the physics effects are dominated by the connection to the wall. The specificity of the ED configuration is that it is an open divertor configuration, with possible neutral sources distributed all around the plasma edge. For the Tore Supra experiments analyzed in this paper, the main plasma characteristics are: deuterium gas, $a = 0.74$ m, $R = 2.41$ m, $B_t = 3.6$ T, $I_p = 1.56$ MA corresponding to an edge safety factor $q_\psi(a) \approx 3$. The outboard carbon limiter is inserted 0.03 m radially ahead of the ED modules. A total input power of up to 6.5 MW is achieved by means of up to 5 MW of ICRH and 1.5 MW of ohmic heating. This corresponds to an average power density close to 0.25 MW/m^3 and a radial power flow to the edge of ≈ 0.09 MW/m^2.

The paper is organized as follows. In Section 2, a simple analysis of the power balance in the edge is used to evaluate the maximum heat flux that is possible to exhaust by radiation. The difficulties in the measurement of the total radiated power are stressed. Section 3 is a review of the main experimental results obtained in the highly radiative edge scenarios. The experiments are classified according to the spatial structure of the edge radiation. In Section 4, the issues governing the choice of the radiating species are discussed: they include the radiation capability, the contamination of the plasma core, and the desired temperature range. The physics effects having an influence on these three issues are reviewed in Sections 4.1, 4.2 and 4.3, respectively. The consequences of the high edge radiation on the energy confinement in the plasma core are summarized in Section 5.

2. Power balance in the edge

The total power radiated by a species Z can be written as

$$P_{rad} = \int n_e n_Z L_Z(T_e)\,dV, \tag{1}$$

where n_e and n_Z are the electron and impurity densities, $L_Z(T_e)$ is the cooling rate, which depends on the electron temperature T_e, and the integration is over the radiating volume. Assuming constant values for n_e, n_Z and T_e in the radiating layer ($n_e = n_{e,rad}$, $n_Z = n_{Z,rad}$, $T_e = T_{e,rad}$). Eq. (1) gives

$$P_{rad} = n_{e,rad} n_{Z,rad} L_Z(T_{e,rad}) V, \tag{2}$$

indicating a linear increase of the radiated power with the densities of electrons and impurities in the radiating volume, with the cooling rate, and with the effective volume dedicated to radiation (V). From Eqs. (1) and (2) we can find out that the power radiated by a species Z is determined both by particle and heat transport, which govern the density and temperature spatial distributions, and by the shape of the cooling rate function in the plane (T_e, L_Z). Therefore, the ultimate goal in the radiating layer scenario is to be able, experimentally, to optimize these three parameters (particle transport, heat transport, and shape of $L_Z(T_e)$) in order to maximize the power radiated by a given species. More insight on the role of heat transport in determining the maximum achievable radiated power can be obtained by writing the radial heat flux balance equation [1,11]:

$$\frac{dQ}{dr} = -n_e n_Z L_Z(T_e) \tag{3}$$

with

$$Q = -\kappa \frac{dT_e}{dr}, \tag{4}$$

where κ is the heat conductivity. From Eqs. (3) and (4) we have

$$Q_1^2 - Q_0^2 = 2\int_{T_0}^{T_1} n_e n_Z \kappa L_Z(T_e)\,dT_e, \tag{5}$$

where Q_1 is the power flux from the plasma core, and Q_0 is the conducted-convected power flux at the limiter surface. T_1 and T_0 are the electron temperatures at the inner boundary of the radiating layer and at the last closed magnetic surface, respectively. Assuming that $Q_0 \approx 0$, the maximum achievable radiated power corresponds to the maximum heat flux that it is possible to exhaust by radiation:

$$P_{rad} = Q_1 S = \sqrt{2\int_{T_0}^{T_1} n_e n_Z \kappa L_Z(T_e)\,dT_e} \times S, \tag{6}$$

where S is the plasma surface area. Therefore, enhancing the heat conductivity also enhances the maximum achiev-

able radiated power. However, Eq. (6) also shows the limit imposed by heat conduction on the effectiveness of exhausting the power by radiation. Indeed, assuming a constant value of n_Z in the radiating layer now gives $P_{rad} \propto \sqrt{n_{Z,rad}}$, to be compared to $P_{rad} \propto n_{Z,rad}$ obtained from a simple analysis. The effects of particle transport, heat transport, and of the shape of $L_Z(T_e)$ on the radiation capability (i.e., the maximum achievable radiated power) of a given species will be discussed further in Section 4.

In analyzing the power balance in the edge, not only radiation losses, but also hydrogen charge-exchange (CX) losses, should be considered. CX losses are as effective as radiation losses in reducing the power load on the target plates since they generate a uniformly distributed power deposition. Moreover, whereas radiation losses affect only the electron heat flux by modifying the electron temperature gradient, CX losses reduce the ion heat flux. CX losses can play a significant role in the power balance of the edge region where the electron temperature is lower than ≈ 5 eV, corresponding to a low ionization rate of hydrogen atoms.

An experimental verification of the power balance equation in the edge needs a measurement of both the radiated, CX and conducted–convected power losses. The radiated and CX losses are measured, without distinction, by means of bolometry. Here, one has to be cautious that the quantity measured by bolometry is not the radiated power loss alone (although this is true in most experimental conditions where CX losses are negligible), but that it is the radiated + CX power losses. An accurate measurement of these losses should take into account their possible toroidal and poloidal asymmetries. It means that several bolometer arrays should be distributed around the torus, and a tomography should be made in a poloidal section. This has been the case only recently in most tokamaks. In TEXTOR first experiments in 1990–1994, only half a poloidal radiation profile was actually measured, and the second half was deduced by symmetrization (following the usual assumption, we now call 'radiation' the quantity measured by bolometry, while keeping in mind the limitation imposed by CX). Recently, a new tomographic bolometer diagnostic has been installed on TEXTOR. This diagnostic consists of three cameras with a total of 40 chords and allows a 2-D reconstruction of the radiation pattern. This system shows for similar discharge conditions a similar general behaviour of the radiation profile than that measured with the old bolometer array. On Tore Supra, a poloidal array of 16 bolometers located on a top port at one toroidal location was used in the experiments reported in this paper. A new poloidal array, identical to the first one, but installed 120° away toroidally, is now also available.

The conducted–convected power deposited on the limiter is measured by infrared cameras. The heat flux to the surface is deduced from the surface temperature evolution, either by solving the semi-infinite wall equation for long thermal time constant systems, or more directly by proportionality to the temperature difference between the surface and the coolant for actively cooled items with sufficiently low thermal time constant.

3. Experimental results and spatial structure of the radiation

In this section the main results obtained in the highly radiative edge scenarios in different tokamak experiments are reviewed, and classified by the spatial structure of the radiation: poloidally symmetrical or asymmetrical layers, radiation being attached or detached from the limiter. Poloidally asymmetrical layers (such as MARFEs or low-field-side radiation observed in the Tore Supra ED configuration) correspond to a region where the physics effects are governed by parallel transport. On the contrary, perpendicular transport effects are dominant in poloidally symmetrical layers. Moreover, the nature of the radiating species also plays a key role in determining the spatial structure of the radiation. These issues will be further discussed in Section 4, and we will now summarize the experimental results.

3.1. Poloidally symmetrical layer: attached plasmas

The best example of a poloidally symmetrical radiating layer in attached plasma conditions is given by the experiments performed in TEXTOR at high heating power density (0.5 MW/m^3) [12]. In these experiments, the tokamak walls are either boronized or siliconized. With these wall conditioning techniques, and at high power density, the radiation level without impurity injection remains low, even at the highest electron densities. The maximum value of P_{rad}/P_{tot} is roughly 0.3 with boronized walls and 0.5 with siliconized walls [13]. Therefore, it is necessary to inject impurities to enhance the radiation level. In TEXTOR, the high radiation losses are triggered by neon ($Z = 10$) or silicon ($Z = 14$) injection, or both. Quasi-stationary operation is obtained by using a feed-back controlled injection system allowing the radiation level to be adjusted to a pre-programmed value. In the case of neon, the sink is provided by the ALT-II pump limiter. In the case of silicon, the tokamak wall itself acts as a pump, since silicon is a non-recycling impurity. In these conditions, a ratio $\gamma = P_{rad}/P_{tot}$ up to 0.9 can be obtained, in a stable radiating layer with no sign of detachment. These experiments are illustrated in Fig. 1 [8]. The plasma is heated with a total of 3.8 MW of ohmic, ICRH, and balanced neutral beam injection. The feed-back controlled neon injection system (monitored by the brightness of a NeVIII line) is ramped up on purpose in order to check the radiation limit. The line averaged central electron density increases from 5 to 6×10^{19} m^{-3} during the high radiation phase, and the diamagnetic energy is close to 120 kJ.

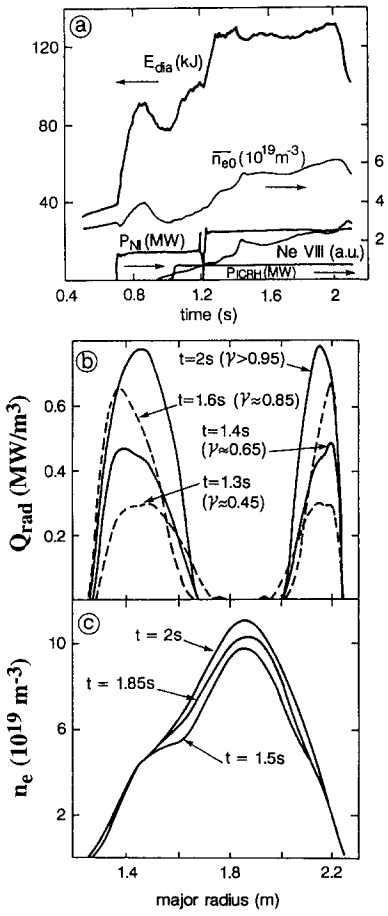

Fig. 1. (a) Time evolution of the diamagnetic energy E_{dia}, line averaged electron density $\overline{n_{e_0}}$, auxiliary heating power, and NeVIII spectral line brightness in a highly radiative edge experiment with neon injection in TEXTOR. Also shown are the radial profiles of the radiated power density (b), and electron density (c) at different times during the rise of neon injection. Adapted from Ref. [8].

The radiated power density profiles are shown in Fig. 1(b). A maximum radiated power density of 0.8 MW/m^3 is reached in the radiating layer, corresponding to a total radiated power of 3.5 MW. The radial extent of the radiating layer is roughly 30% of the minor radius. The central concentration of the injected impurity remains low: n_{Ne}/n_e measured by charge exchange recombination spectroscopy or by visible 'bremsstrahlung' is lower or of the order of 1%. In the case of silicon injection, the central concentration n_{Si}/n_e is even lower. The electron density profiles (Fig. 1(c)) are peaked, of the supershot type (due to NBI auxiliary heating). A striking feature that has to be noted is that, in these experiments, the $q = 2$ surface is located in the highly radiating region. However, the discharge remains MHD stable.

Similar experiments are reported from Tore Supra, when the limiter configuration is used [7]. In these experiments, however, the heating power density is lower than that of TEXTOR experiments (≈ 0.2 MW/m^3 obtained through 3.5 MW of ICRH and 1.5 MW of ohmic heating). The tokamak walls are boronized. The volume averaged electron density is close to 4.5×10^{19} m^{-3}, and the radiation level due to intrinsic carbon is $P_{rad}/P_{tot} \approx 0.4$. Neon injection is used to enhance the radiation. The radiation profile is poloidally symmetrical and the plasma remains attached to the limiter up to $P_{rad}/P_{tot} \approx 0.7$, corresponding to 9.0×10^{19} injected neon atoms. Only a small fraction of the injected neon penetrates into the confined plasma where the neon concentration deduced from spectroscopic and visible 'bremsstrahlung' measurements is $n_{Ne}/n_e \approx 0.9\%$. For a higher neon injection level (up to 12×10^{19} injected atoms corresponding to $P_{rad}/P_{tot} \approx 0.8$) a high-field-side MARFE is formed, and an even higher injection leads to a disruption.

3.2. Poloidally symmetrical layer: detached plasmas

In the limiter configuration, detachment from the limiter occurs when the edge electron temperature falls below the threshold for ionization of all plasma species, including deuterium. Consequently, a neutral shield is formed at the edge, and the radiating layer is shifted towards a smaller minor radius. In a detached plasma, most of the power input is radiated in a poloidally symmetrical shell, and the power and particle fluxes to the limiter are reduced by a large factor. The first detached plasmas were reported in TFTR in 1985 [14,15] in ohmically heated experiments. In these experiments, the plasma is detached from the limiter by reducing the plasma current while simultaneously injecting cold neutral deuterium gas. All of the ohmic power eventually appears as radiation. The influence of neutral beam auxiliary heating on detached plasmas was then investigated on TFTR from 1989 [16]. This is probably the first attempt to produce a radiative mantle in a controlled fashion, and with auxiliary heating power. The experiment consists in producing a detached plasma, and then heating the plasma with neutral beam auxiliary power. As the heating power is increased above 2 MW and without simultaneous gas puffing, the plasma radius expands until reattachment occurs. However, deuterium or neon puffing allows to maintain detachment at powers of over 5 MW. Fig. 2 shows the radiated power density profiles for detached plasmas with 1.75 MW of beam power and simultaneous puffing of deuterium, and with 4.85 MW of beam power and simultaneous puffing of neon. Interestingly enough, the maximum value achieved for the radiated power density (0.8 MW/m^3) is the same as that obtained in TEXTOR high heating power density radiative plasmas. Also, the plasma minor radius in the TFTR detached plasma is decreased to a value close to that of TEXTOR attached plasmas (≈ 0.46 m), so that the radiation profiles are very similar in TEXTOR and TFTR. The higher total

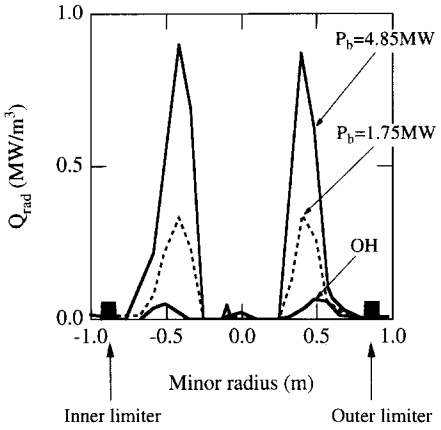

Fig. 2. Radiated power density profiles for beam heated detached plasmas in TFTR [16]. Three levels of heating power are shown: ohmic, $P_b = 1.75$ MW and $P_b = 4.85$ MW.

radiated power in TFTR (≈ 5 MW compared to ≈ 3.5 MW in TEXTOR) is only due to its larger major radius. To our knowledge, the highest achieved total radiated power in a detached plasma — close to 20 MW — has been obtained in the JET limiter configuration [17]. Indeed, using the carbon belt limiters, and with up to 20 MW of ICRH and NBI heating power, the impurity influx can be so large that detachment occurs spontaneously. However this detached phase is not controlled, and a transition to a MARFE is eventually observed after typically 0.5 s. This result, together with the TFTR experiments, shows that as increased additional heating is applied, it gets progressively more difficult to obtain detachment.

In TEXTOR, detached plasmas are obtained only at low power density (0.035 MW/m^3, pure ohmic heating) and in boronized conditions, the radiating species being either intrinsic carbon at high electron densities, or injected neon [18]. In these conditions, detachment occurs usually before γ reaches 0.5 to 0.6, compared to over 0.9 at high heating power density. In Tore Supra, stable detached plasmas are also obtained at low power density, close to the density limit, when the ergodic divertor is activated [19]. In this case, the radiating impurities are intrinsic carbon, oxygen and/or chlorine.

3.3. Poloidally asymmetrical layer: stable MARFE

A MARFE (multifaceted asymmetric radiation from the edge) is a toroidally symmetric, poloidally asymmetric luminous band occurring within the last closed magnetic surface at the high-field-side edge of the plasma [20]. MARFEs are generally observed close to the density limit, in high power density plasmas. The radiated power in a MARFE can be approximately equal to the input power, the radiated power density in a MARFE being several times higher than in a detached plasma [16,21]. However, MARFE phenomenons are generally not stable. They are the manifestation of a thermal instability, with impurity radiation being the main energy loss mechanism out of the MARFE volume. Yet, a stable MARFE has been observed in JET discharges run on the beryllium belt limiter with a beryllium evaporation coating on the walls [22,23]. This MARFE appears when the density limit is reached, and it prevents any further increase in density. Almost all of the 10 MW input power is radiated in the MARFE volume, chlorine being the dominant radiating species. The specific feature of these discharges is that they are almost never disruptive, and in many cases the MARFE extinguishes, after which the bulk plasma density recovers to its pre-MARFE value, and the entire cycle is repeated once or several times.

3.4. Poloidally asymmetrical layer: low-field-side radiation

In Tore Supra ED configuration plasmas, stable operation with a high radiation level in the edge is obtained when radiation is located on the plasma low-field-side (LFS). Experiments are reported in Refs. [6,7,24]. We will summarize here the main results. A radiated fraction $\gamma = P_{rad}/P_{tot}$ in the range 0.8–0.9 is obtained with neon injection. The radiated power can be as high as 5.5 MW for a total input power of 6.5 MW achieved by means of 5 MW of ICRH and 1.5 MW of Joule heating. The volume averaged electron density is 3.2×10^{19} m^{-3}. The radiated fraction before neon injection, is $P_{rad}/P_{tot} \approx 0.5$. However the effective charge is low, close to 1.3. Less than 2.0×10^{19} injected neon are enough to bring the radiative fraction in the 0.8 range. The line integrated radiation emissivity profile is shown in Fig. 3. This line integrated profile is not straightforward to interpret because of the ergodicity of the edge layer. Indeed, a high line integrated radiation on a given edge chord can be due to the fact that the chord

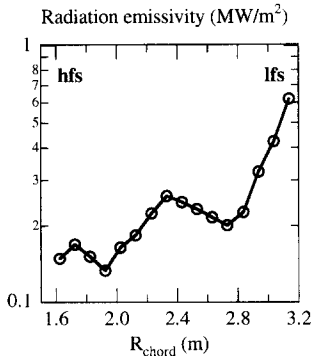

Fig. 3. Line integrated radiation emissivity profile in Tore Supra highly radiative edge experiments in the ED configuration with neon injection. In this particular discharge, $P_{rad}/P_{tot} = 0.8$ corresponding to a total radiated power of 3.5 MW. Radiation is located on the plasma low field side (LFS).

intercepts a flux tube connected with a short connection length to one ED module. A model including the description of the exact magnetic topology in the edge should be used to unfold an accurate two dimensional map of the radiation emissivity. However, one can say that, globally, radiation is located on the plasma LFS, close to the ED modules where the main plasma–surface interaction takes place. The maximum value of the radiated power density can be estimated to be close to 0.7 MW/m^3, which is of the same order of magnitude as that measured in TEXTOR. The plasma remains attached for γ up to 0.8–0.9. The neon concentration (n_{Ne}/n_e) in the plasma core remains low, close to 0.8%.

For higher values of γ, the plasma detaches from the LFS, and a radiation 'swing' is observed: a high-field-side (HFS) MARFE is formed, and a disruption generally occurs. This observation shows the limitations of the forced radiating edge scenario: the stability of the radiating layer is controlled as long as the radiation remains confined to the ED proximity. As soon as the HFS MARFE develops, the stability of the layer is lost. The same observations are made in radiative divertor experiments in JET or DIII-D, when the divertor MARFE extends close to the main plasma [25]. Experiments have been performed in Tore Supra, demonstrating that it is possible to prevent the radiation swing to occur. In these experiments, a highly radiating edge plasma is produced using neon injection, together with deuterium injection. The deuterium injection is feed-back controlled by the LFS radiation signal. When this signal drops under a given threshold, the deuterium injection is stopped and the radiation remains located on the plasma LFS.

4. Issues governing the choice of the radiating species

The conditions for obtaining a highly radiative region at the plasma edge are tied closely to the density limit conditions. The goal of the radiative edge scenarios is to run a stable plasma at a point in the operational space close to where the density limit disruption would occur. This is why the question of the stability of the highly radiative edge layers is so crucial. The ultimate symptom that the density limit is reached is always a very high radiation level in the edge. This causes the temperature profile to contract, leading to a current profile that is MHD unstable. Experimentally, there are two methods for approaching the density limit conditions. The more straightforward path consists in increasing the electron density through deuterium injection. The other path is to operate at a given electron density, and adjust the density limit value through the low-Z impurity level. This is the technique used in TEXTOR and Tore Supra in the neon injection experiments. In both cases, radiation comes either from impurity line emission (intrinsic or injected impurity), or from hydrogen line emission.

If the choice is made to use an impurity injection technique, the question is raised of what impurity species is the most appropriate. The issues that should be considered for the choice of the impurity species are discussed in the following: radiation capability (Section 4.1), contamination of the plasma core (Section 4.2), and desired temperature range (Section 4.3).

4.1. Radiation capability

Impurity line radiation and hydrogen radiation are the two potential atomic processes that can be used to radiate the power in the edge. Charge exchange losses through the H^+–H^0 collisions are also generally considered as a promising process to spread out the heat at the plasma edge. However, radiation is not involved here, but momentum transfer between the energetic H^+ ions and the cold hydrogen neutrals. Therefore this process is not under the scope of this paper. In this section, our goal is to discuss what atomic species is the most appropriate to maximize the radiated power in the edge, and to discuss the physics effects governing the radiation capability of a given species.

High Z impurities would be the best suited to maximize the radiated energy per impurity particle. But radiation should be restricted to the plasma edge, which means that the impurity should be either completely ionized, or in the H-like or He-like ionization stages in the plasma center. For the central electron temperatures typical of present tokamaks, this criterion limits the impurity charge number to that of argon. Practically, C, N, O, Ne, Si, Cl and Ar have been tested. For a given impurity species, atomic processes and transport effects in the plasma edge determine the maximum achievable radiated energy per impurity particle.

4.1.1. Coronal equilibrium

The power radiated by a species Z is given, to first order approximation, by the coronal equilibrium calculations for the cooling rate $L_Z(T_e)$. In the coronal model, particle transport effects are neglected, and the impurity charge state distribution is determined by the balance between ionization and recombination. A review of recent developments in the computation of the atomic rate coefficients needed to calculate $L_Z(T_e)$ can be found in Ref. [26]. The maximum value of $L_Z(T_e)$ increases from $\approx 3 \times 10^{-32}$ W m^3 for beryllium, to $\approx 3 \times 10^{-31}$ W m^3 for argon. A specific feature of the cooling rate functions from the coronal equilibrium model is that they are peaked at a given electron temperature, corresponding to the existence of ionization stages equal or lower than the Li-like ions. This temperature is $\approx$ 2–3 eV for beryllium and $\approx$ 30 eV for neon. Therefore, in the coronal model approximation, radiation is restricted to a narrow temperature range, and this temperature is higher for higher Z elements. However, for the experimental conditions prevailing at the edge of tokamak plasmas, two important physics effects have to be

included and modify the coronal equilibrium predictions: transport and charge exchange processes.

4.1.2. Edge particle transport processes

In the plasma edge, the typical time to approach coronal equilibrium (τ_{cor}) is longer than the particle transit time due to diffusion processes (τ_p). Indeed, the latter is of the order of $\Delta^2/D_\perp \approx 1$–$10$ ms, where Δ is the typical radial dimension of the edge region and $D_\perp$ is the particle diffusion coefficient in this region. The time constant to reach coronal equilibrium (τ_{cor}) is larger than τ_p because of the slow recombination processes. Depending on the precise edge conditions, τ_{cor} can be 0.1 s or longer. Therefore the impurity charge state distribution is determined by the balance between ionization and transport processes. The result can be quite distinct from that found in the coronal model: the dominant charge state at a given electron temperature is generally lower than that given by the coronal equilibrium, because ions are rapidly transported from colder to hotter regions of the plasma. In these conditions, the following expression for the total radiated power is introduced [27]:

$$P_{rad} = E_{rad}\Gamma_Z, \tag{7}$$

where Γ_Z is the total flux of the impurity particles of atomic number Z entering the plasma, and E_{rad} is the radiation potential. E_{rad}, like the coronal equilibrium cooling rate $L_Z(T_e)$, represents the radiated energy per impurity particle, with the difference that E_{rad} includes edge transport effects. The relation between E_{rad} and L_Z can be derived from a simple one dimensional model [28]. Indeed, the impurity density in the radiating layer can be written as

$$n_{Z,rad} = \frac{v_0}{\langle\sigma v\rangle^i_0 n_{e,b}}\frac{\Gamma_Z}{D_{\perp,b}}, \tag{8}$$

where v_0 is the velocity of the incoming neutrals, $\langle\sigma v\rangle^i_0$ their ionization rate coefficient, $n_{e,b}$ the electron density in the boundary layer where ionization of impurity neutrals occurs, and $D_{\perp,b}$ the particle diffusion coefficient in this layer. The radiating volume is $V = 4\pi^2 aR\delta$, $\delta = \sqrt{D_\perp/\langle\sigma v\rangle^i n_{e,rad}}$ being the radial width of the radiating shell ($D_\perp$ is the particle diffusion coefficient in the radiating layer, and $\langle\sigma v\rangle^i$ is the ionization rate coefficient of the radiating ions, i.e., generally the Li-like ions). Eq. (2) can then be written in the form

$$P_{rad} = 4\pi^2 aR\frac{\sqrt{n_{e,rad}}}{n_{e,b}}\frac{v_0}{\langle\sigma v\rangle^i_0\sqrt{\langle\sigma v\rangle^i}}\frac{\sqrt{D_\perp}}{D_{\perp,b}}L_Z\Gamma_Z \equiv E_{rad}\Gamma_Z. \tag{9}$$

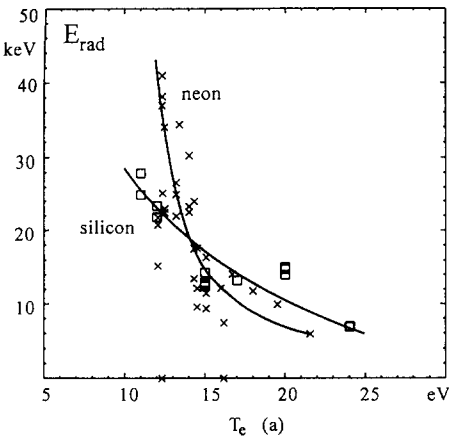

Fig. 4. Radiation potential versus edge T_e, measured in TEXTOR for neon and silicon impurities [13].

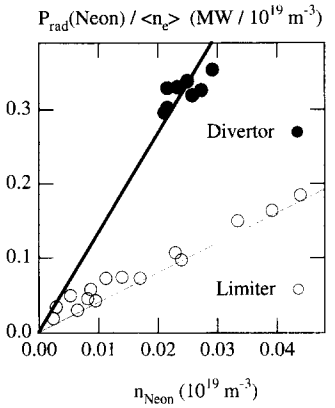

Fig. 5. Radiation capability of neon in the limiter (open circles) and ED (closed circles) configurations in Tore Supra.

E_{rad} has been measured in TEXTOR for several impurities by measuring both P_{rad} and Γ_Z. Fig. 4 gives the radiation potential for neon and silicon as measured in the TEXTOR experiments. Whereas, as already discussed, the coronal equilibrium cooling rate functions $L_Z(T_e)$ are sharply peaked for a given electron temperature, the radiation potential increases steadily as T_e is decreased. This can be understood from Eqs. (8) and (9): a decreased edge temperature corresponds to a decreased ionization rate coefficient $\langle\sigma v\rangle^i_0$, thus an enhanced penetration of neutral atoms producing, in our model, an enhanced impurity density $n_{Z,rad}$. A reduced electron temperature also corresponds to a wider radiating shell (larger value of δ). Also, whereas the cooling rate for silicon is higher than that of neon, due to a higher charge number Z, the radiation potentials of the two species are almost the same. Again, this is due to the larger penetration of neon compared to that of silicon, producing a larger neon density for a given flux in the edge Γ_Z.

Evidence of the effect of particle transport in the edge on the radiation capability of impurities is also found in Tore Supra, when comparing highly radiative edge experiments in the limiter and ED configurations. In these experiments, the measurement of the total neon flux at the

plasma edge (Γ_{Ne}), and thus the measurement of the radiation potential of neon is not available. Consequently, the radiation capability of neon is defined by the volume integrated cooling rate function:

$$\frac{P_{rad}(\text{neon})}{\langle n_e \rangle \langle n_{neon} \rangle} = \int L(T_e)\,dV, \qquad (10)$$

where $\langle n_{neon} \rangle$ is the volume averaged total neon density in the plasma core, deduced from spectroscopic, soft X-rays and visible 'bremsstrahlung' measurements. P_{rad}(neon) is the power radiated by neon in the edge, estimated from the peripheral NeVII (55.8 nm) line brightness. The radiation capability of neon has been measured both in the ED and limiter configurations. The result is shown on Fig. 5 where the radiation capability of neon is indicated by the slope of the two lines. It is three times higher in the ED case than in the limiter one, i.e., for a given neon density in the plasma core, the neon radiation is three times higher in the ED configuration than in the limiter one. This increase of radiation for a given amount of impurity density in the plasma is the signature of either a strong decrease of the confinement time in the divertor volume (thus indicating a departure from the coronal equilibrium model), or a more favourable edge temperature profile for NeVII line emission. The latter is possible from the theory of the stochastic edges which predicts a flattening of the edge temperature gradient in the ergodic region [10]. However, the measurement of the actual edge electron temperature profile is not available in the neon injection experiments. In order to further distinguish between the two possible causes for the enhanced radiation capability of neon in the ED configuration, the experiments have been modelled with the transport code RITM [29,30]. This code computes self-consistently the density and temperature profiles of electrons and of background and impurity ions. Transport processes in a stochastic boundary are described on the basis of simple analytical models. The main result of the analysis with RITM is that both an increased particle transport in the ergodic region, and a flattening of the edge temperature profile are needed to explain the observations, and that they produce the same contribution to the enhancement of the neon radiation capability. An increase of the particle diffusion coefficient in the ED region (by a factor of approximately three, roughly within the completely stochastic region where a flat T_e profile is expected) is also required to correctly simulate the intensity ratio of two carbon spectral lines, $\rho = Ly\alpha/R_{CV}$, with the Tore Supra impurity transport code [31] (Fig. 6, see following section).

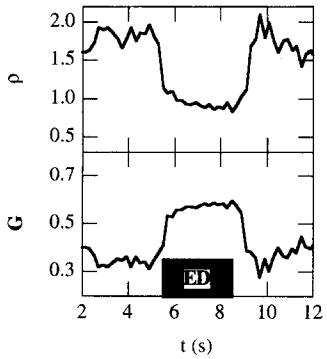

Fig. 6. Time evolution of the carbon line intensity ratios ρ and G, in Tore Supra ED experiments. The ED is switched on at $t = 5.5$ s. The decrease of the ρ ratio indicates an increase of the particle diffusion coefficient in the ergodic region. The increase of the G ratio is indicative of a large neutral deuterium atom density in the same region.

4.1.3. Charge exchange processes

Charge exchange recombination, as edge particle transport, modifies the coronal equilibrium cooling rate functions $L_Z(T_e)$ by altering the ionization distribution toward lower charge states which radiate more strongly [26]. For charge exchange recombination to be high enough, a large hydrogen neutral density is required in the edge. In Tore Supra, although no direct measurement of the edge hydrogen neutral density is available, evidence of the importance of CX processes in ED plasmas is demonstrated by spectroscopic measurements. Two carbon spectral line intensity ratios, $\rho = Ly\alpha/R_{CV}$ and $G = I_{CV}/R_{CV}$ ($Ly\alpha$ = CVI 33.74 Å, R_{CV} = CV 40.27 Å, resonance line, and I_{CV} = CV 40.73 Å, intercombination line) are measured both in the limiter and ED configurations [32]. Fig. 6 shows the time evolution of the two ratios in an experiment where the ED is switched on at $t = 5.5$ s. The ρ ratio is an indication of the relative amounts of H-like and He-like carbon ions. Therefore, it is mainly sensitive to the particle transport in the edge, and it decreases as a consequence of increased particle diffusion coefficient (Section 4.1.2). The G ratio is, at tokamak electron densities, an inverse function of the electron temperature, if electron collisions are the dominant process populating excited states. For a given electron temperature, it is increased by CX recombination of H-like carbon ions. The G ratio has been modelled in the ED configuration (experimental value $G_{exp} = 0.6$) with the Tore Supra impurity transport code [31], and using the measured value of the edge electron temperature. The calculated value, if CX is neglected, is in the range 0.3–0.4, depending on the exact electron temperature at the radial position where the CV ion emitting shell is located. In order to approach the experimental value of 0.6, it is necessary to assume the existence of a large peripheral neutral deuterium density n_0, in the 10^{16} m^{-3} range at the CV emitting layer ($r/a = 0.85$), and in the 10^{17} m^{-3} range at $r/a = 1$.

Charge exchange processes are beneficial for the highly radiative edge scenarios because they can extend the radiation to regions with much higher electron temperature values, thus increasing the effective volume available for

radiation, as far as the hydrogen neutral density remains large in this volume. In this respect, the spatial localization of hydrogen neutrals is a key issue. It is determined by the geometry of the device, limiter, open divertor (such as ED), or X-point divertor configurations, open divertors being probably the best suited to maximize CX effects since the corresponding neutral sources are widely distributed on a large surface area.

4.2. Contamination of the plasma core

The second issue controlling the success of the highly radiative edge scenarios is that the impurity concentration in the plasma center should remain below a critical value. Above this critical value, ignition is not possible, due to too large 'bremsstrahlung' losses or fuel dilution. The maximum allowed impurity fractions for ignition decrease with increasing Z. For ITER, it is estimated that the central impurity fraction must be strictly limited to give $Z_{\text{eff}} \leq 1.6$ [33]. Therefore, the impurity level should be as high as possible in the edge to obtain a high radiation level there, and as low as possible in the plasma center. Screening effects, radial particle transport in the edge and pumping effects determine the impurity density radial profile and the induced contamination of the plasma core.

4.2.1. Screening effect

The screening effect is defined by the fact that ionization occurs in the edge low confinement region, i.e., the SOL of the limiter configurations, or the laminar zone of the ED configuration. Ionization in the low confinement region is possible if the radial extent of this region exceeds the impurity ionization length. For the screening effect to be beneficial for the highly radiative edge scenarios, not only impurities have to be ionized in the low confinement region, but also they have to radiate as much as possible in this region. The screening effect can be investigated by comparing the ionization length for a given species and the width of the low confinement zone. This has been done for comparison with Tore Supra experiments, the width of the low confinement zone (λ_{screen}) being taken equal to the width of the laminar zone ≈ 0.06 a [10]. The ionization length is

$$\lambda_i = \frac{v_0}{\langle \sigma v \rangle_0^i n_e}, \tag{11}$$

where v_0 is the velocity of the incoming neutral, $\langle \sigma v \rangle_0^i$ the ionization rate coefficient for the given species, and ne the local electron density. The results are shown in Fig. 7 [10] where the ratio $\lambda_{\text{screen}}/\lambda_i$ is plotted as a function of T_e, for an electron density $n_e = 1 \times 10^{19}$ m^{-3}. The impurity species for which $\lambda_{\text{screen}}/\lambda_i > 1$ are efficiently screened. In evaluating λ_i, various neutral energies have been used in relation to the most likely generation mechanism. In the case of noble gases, He, Ne and Ar, we have

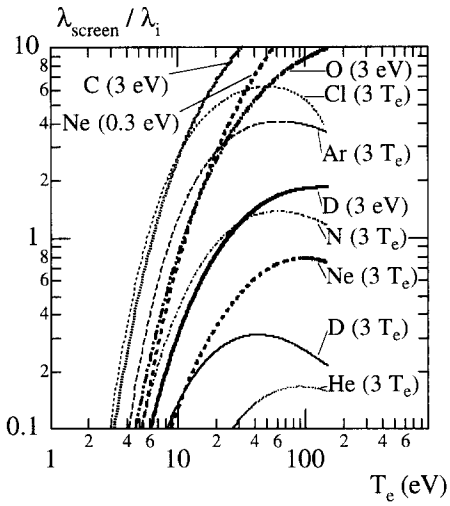

Fig. 7. Screening ratio $\lambda_{\text{screen}}/\lambda_i$ [10], for different impurity species, and different neutral energies. $3T_e$ corresponds to backscattered neutrals, 3 eV to a chemical generation process, and 0.3 eV to thermal desorption from the wall. $(\lambda_{\text{screen}}/\lambda_i) > 1$ corresponds to an efficient screening effect.

considered that the backscattering energy is the most appropriate. This energy is in the range of $T_i + 3T_e$, hence very dependent on the plasma edge conditions (the term $\approx 3T_e$ is the energy transferred from the electrons to the ions in the sheath). In fact, it has been observed for neon that only a small fraction of the neutrals are characterized by these energies [34]. The measured velocity for the largest fraction of neon neutrals is typically 0.3 eV. For C, O and N, both backscattering and chemical production mechanisms can be important. In the case of chemical production, the chemical energy of the molecule is shared on the separate atoms during the dissociation process. This ensures a minimum energy of about 3eV to the neutrals. In Fig. 7, the chemical generation is illustrated by C and O while the backscattering mechanism is given by N (the ionization rate coefficients of C, O and N are roughly equal, so that the ionization length of backscattered nitrogen is roughly the same as that of backscattered carbon or oxygen). Regarding chlorine, only the backscattering process allows for values of $\lambda_{\text{screen}}/\lambda_i$ within the range of interest. Fig. 7 shows that only backscattered impurities exhibit a significant penetration probability. The impact of the production mechanism on the impurity penetration depth has also been analyzed in Ref. [35].

Let us now compare the predictions of this simple model to the experimental results obtained in Tore Supra. In Tore Supra, the central carbon density is reduced by a factor of 5 in the ED configuration with respect to the limiter configuration [10]. The decrease of the edge electron temperature due to the stochastic boundary can contribute to this result both through a lowering of the source

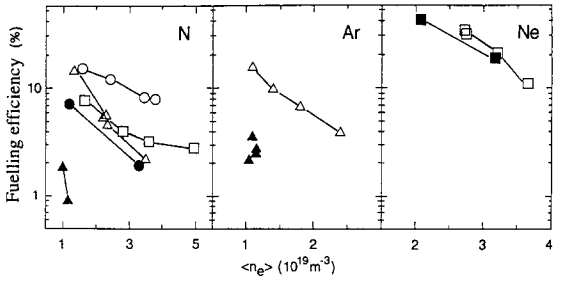

Fig. 8. Fuelling efficiency (ratio of the bulk content to the total injected quantity) of nitrogen, argon and neon in Tore Supra limiter (open symbols) and ED configurations (closed symbols), as a function of the volume averaged electron density. Triangles deuterium plasmas, carbonized walls. Circles: helium plasmas, carbonized walls. Squares: helium plasmas, boronized walls.

and a lowering of the energy of the backscattered neutrals. The same results are found for oxygen, but only when the oxygen density is normalized to the hydrogen flux given by H_α measurements. Chlorine, as predicted by the high value of $\lambda_{screen}/\lambda_i$, is strongly reduced in the ED configuration. However, it is difficult, through the analysis of the behaviour of intrinsic impurities, to determine whether the observed decontamination effect in the ED configuration is due primarily to a reduction of the source of impurities or to a reduced ionization length corresponding to a high value of $\lambda_{screen}/\lambda_i$. Therefore, short puffs of gaseous impurities have been injected in Tore Supra [36]. The fuelling efficiency measured for N, Ar, and Ne are plotted in Fig. 8. In all cases, the fuelling efficiency decreases with increasing density. For N and Ar, a further decrease by a factor of 5 is obtained with the ergodic divertor. In helium shots, neon behaves in the same way for limiter and ergodic divertor configurations. Furthermore, its measured penetration probability is large. The results for nitrogen agree with the predictions of Fig. 7, i.e., nitrogen is efficiently screened, provided that chemical generation is the dominant generation process for nitrogen neutrals. Ar also is strongly screened as expected from Fig. 7. On the contrary, the results for Ne indicate that only the back scattered neon atoms determine the neon penetration. As a conclusion for this section, one finds that as far as the screening effect is concerned, the most appropriate impurity species for the highly radiative edge scenario is the one that maximizes the ratio $\lambda_{screen}/\lambda_i$, for example N or Ar.

4.2.2. Radial particle transport

Radial particle transport processes inside the separatrix determine the radial distribution of impurity ions. This distribution can possibly be hollow, which is the best achievable for the purpose of highly radiative edges. The effect of the transport processes inside the separatrix are illustrated by the neon density radial profiles obtained in TEXTOR during the radiative edge cooling experiments [8]. These profiles are flat, in strong contrast with what is predicted by the neoclassical theory. The neoclassical theory predicts that the impurity density radial profiles should be of the form $(n_i)^Z$, where n_i is the main plasma ion density and Z is the impurity charge number. However, in TEXTOR, hollow Z_{eff} profiles are obtained, due to the very peaked electron density profiles. Also in JET, hollow neon and carbon density profiles have been reported both in L and H mode [37], the profiles remaining hollow even during substantial edge fuelling. These flat or hollow impurity density profiles are attributed to a convection velocity directed outwards in the major part of the profiles. The physical reasons for the existence of this convection velocity are not yet well understood.

4.2.3. Pumping

The recycling properties of the impurity species, connected with the pumping capabilities of the device, have also an influence on the contamination of the plasma core. Indeed, a not pumped impurity (i.e., completely recycling), eventually contaminates the plasma core. Stationary discharges with a high radiation level in the edge are only possible with a very well controlled impurity level. In the case of TEXTOR, the ALT-II pump limiter is used as a sink for neon impurity. A feed back system on the neon injection is used [5] to maintain a constant neon level in the plasma. In Tore Supra, active pumping is not yet available for neon.

4.3. Desired temperature range

The third issue for the success of the highly radiative edge scenario (the first issue is a high radiation in the edge, Section 4.1, the second one is a low contamination of the plasma core, Section 4.2) is to be able to control the temperature range in which radiation will occur. This issue is closely related to that of the control of detachment. In the coronal equilibrium approximation, the radiated energy per impurity particle is sharply peaked for a given value of the electron temperature, indicating that, for a given impurity, radiation is restricted to a narrow temperature range. In fact, as already pointed out, edge particle transport processes and CX recombination processes both contribute to increase the size of the temperature window in which a given Z impurity radiates strongly. The choice of the impurity species determines the choice of the temperature window. Neon, for example, radiates at higher T_e than lower Z impurities like carbon and oxygen do. The discussion of the appropriate temperature for radiation is further complicated by the fact that radiation also lowers the temperature. So, the relevant point is to know at what value will radiation bring the temperature in the edge. This value is determined by the power balance in the edge. It is important to predict this equilibrium value of the edge T_e, since a very low edge temperature gives rise to detachment phenomena. Detachment is attractive because most of the power input to the plasma is then radiated in a poloidally

symmetric shell, and the power and particle fluxes to the limiters are reduced by a large factor. However, detachment presents three major drawbacks: (1) a detached state is generally not stable, because the radius of the radiating layer shrinks, and when the $q = 2$ surface is perturbed MHD instabilities are generally excited; (2) when auxiliary heating is achieved with waves (as in Tore Supra, where ICRH is mostly used), the wave coupling efficiency is highly affected by the neutral 'shield' in the edge; (3) the particle exhaust capability by means of throat devices is strongly reduced when the plasma detaches [38]. It results that the best possible scenario is one in which 100% of the power input to the plasma is radiated in a poloidally symmetrical shell, without detachment. It means that the radiating impurity should be chosen such that the equilibrium temperature in the edge is large enough to allow ionization of deuterium neutrals.

5. Consequences on energy confinement in the plasma core

In Tore Supra, no influence of neon injection on the global energy confinement is recorded. The kinetic energy stored in the electrons is in good agreement with the Rebut–Lallia–Watkins predictions, both in limiter and ED configurations, and with or without neon injection.

On the contrary, in TEXTOR, improved confinement conditions are obtained at high electron densities (central line averaged density $\overline{n_{e_0}} \geq 4.0 \times 10^{19}$ m^{-3}) in the radiatively cooled plasmas, with respect to the results obtained in similar conditions without radiation cooling. This is shown on Fig. 9 where the diamagnetic energy is plotted as a function of $\overline{n_{e_0}}$, for discharges with and without radiation cooling. Note that in the discharges without radiation cooling, the diamagnetic energy decreases with increasing $\overline{n_{e_0}}$, whereas it is roughly constant in discharges with a highly radiative edge. For a line averaged density of 5.0×10^{19} m^{-3}, the energy confinement is improved by a factor up to 1.5 in the radiatively cooled plasmas as compared to non-radiatively cooled discharges. Transport analysis [39] show that the enhanced confinement is due to a peaking of the current density profile, resulting from the decrease of the edge electron temperature in the presence of radiation cooling. The improved confinement is also generally linked to a peaked electron density profile. However, experiments in TEXTOR show that two identically peaked density profiles can correspond to different confinement times.

Recently, the compatibility of a radiative boundary with high energy confinement in the plasma core has been demonstrated in ASDEX-upgrade, an X-point divertor tokamak. In these highly radiative edge experiments, new confinement regimes, such as CDH (completely detached H-mode) or improved L-mode, have been established [40]. A key element for entering these regimes is simultaneous puffing of neon and deuterium gas, both carefully feed-back-controlled by the radiated power and the divertor neutral gas flux. Whereas the CDH mode is linked to a modification of the ELM characteristics, and therefore is more specific of X-point divertor experiments, the radiative edge improved L-mode observed in ASDEX-upgrade is probably closely related to the improved confinement mode observed in high density radiatively cooled plasmas in TEXTOR.

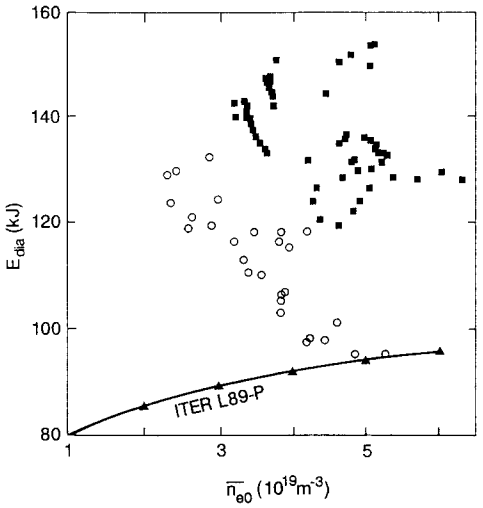

Fig. 9. Diamagnetic energy versus central line averaged electron density for discharges with radiation cooling (siliconized walls, closed squares) and without radiation cooling (boronized walls, open circles) in TEXTOR. The discharges are heated with 3 MW of balanced neutral beam injection. The predictions of the ITERL89-P scaling are also shown. Adapted from Ref. [8].

In conclusion, all these improved confinement scenarios are generally obtained in conditions of peaked electron density and current density profiles, when auxiliary heating is achieved, at least partly, by neutral beam injection. The fact that improved performances have not yet been observed in Tore Supra highly radiative edge experiments can be due to the use of ICRH for auxiliary heating, instead of neutral beam injection.

6. Conclusion

It is now generally recognized that the next tokamak generation (ITER) will require, because of technological limitations of the acceptable power loads on the plasma-facing components, a highly radiating scenario (having the advantage of a more homogeneous power load). It is also clear that this cannot be obtained by intrinsic impurities when using low-Z plasma-facing components. Although most of the present tokamak work addresses the physics of axisymmetric divertors, TEXTOR and Tore Supra experiments have shown that the required conditions can possibly be achieved also in the limiter configuration and with an (open) ergodic divertor. In this paper, we have reviewed

experiments aimed at obtaining highly radiating plasmas in these last two configurations; this requires the injection of extrinsic impurities. Indeed, the obtention of highly radiating homogeneous peripheral layers requires that the peripheral radiation capability be maximized, while at the same time avoiding the plasma core contamination. It is also necessary to insure the stability of the radiating layer, which generally requires that its extension does not reach the $q = 2$ radius (but TEXTOR has shown that this is not apparently an absolute requirement), thus limiting the useful radiating volume. Note that there is a subtle interplay between the radiation capability and the peripheral T_e value, since they influence each other (an increase of the radiation losses decreases the peripheral temperature).

The necessity of an homogeneous radiating layer restricts the use of intrinsic impurities in present day carbon plasma-facing component tokamaks, since low-Z impurities not only need peripheral temperatures which are probably too low, but also have their radiating ions (Li-like) not yet spread out sufficiently to assure a poloidally and toroidally homogeneous radiating layer. On the other hand, high-Z impurities require large T_e values for maximum radiation (thus resulting in large sputtering yields), and also result in large central line radiation, and 'bremsstrahlung', losses. For these reasons, the range of useful radiators is probably limited to argon, neon being one of the best suited (and more used) elements (note that given the T_e value needed by neon, even in the axisymmetric configuration the added radiation extends inside the separatrix; the issues discussed in this paper are therefore relevant also for this configuration).

Tore Supra and TEXTOR plasmas have achieved radiation levels up to 80–90% of the injected power, in steady state conditions. Both experiments have pointed out the necessity of an efficient pumping system to control the radiating layer, and have shown no loss of the plasma confinement properties (even improved confinement in TEXTOR). In Tore Supra, the ergodic divertor has resulted in a three times higher neon radiation capability (for the same central plasma contamination), and permitted to radiate up to 5.5 MW. While the experiments discussed here have shown that the radiating scenario can be obtained in the limiter and ED configurations (with relevant values of the edge heat flux), further confirmation of the possibility to radiate large amounts must wait for the use of more relevant additional power levels (as in Tore Supra, where the ED neutralizers have been modified to permit the extraction of larger conducted–convected powers).

Acknowledgements

The authors wish to thank the TEXTOR Team and Tore Supra Team for providing excellent experimental conditions and valuable data.

References

[1] D.E. Post et al., Phys. Plasmas 2 (1995) 2328.
[2] The JET Team, presented by M. Keilhacker, Plasma Phys. Control. Fusion 37 (1995) A3.
[3] S.L. Allen, A.S. Bozek et al., Plasma Phys. Control. Fusion 37 (1995) A191.
[4] A. Kallenbach, R. Dux et al., Nucl. Fusion 35 (1995) 1231.
[5] U. Samm, G. Bertschinger et al., Plasma Phys. Control. Fusion 35 (1993) B167.
[6] Equipe Tore Supra, presented by A. Grosman, in: Proc. 15th IAEA Int. Conf. on Plasma Phys. and Controlled Nucl. Fusion Res., Vol. 1, Seville, 1994 (IAEA, Vienna, 1995) p. 601.
[7] A. Grosman, P. Monier-Garbet et al., J. Nucl. Mater. 220–222 (1995) 188.
[8] A.M. Messian, J. Ongena, U. Samm et al., Nucl. Fusion 36 (1996) 39.
[9] A. Samain, A. Grosman et al., J. Nucl. Mater. 111&112 (1982) 408.
[10] Ph. Ghendrih, A. Grosman and H. Capes, Plasma Phys. Contr. Fusion (1996), report EUR-CEA-FC-1571, to be published.
[11] H. Capes, Ph. Ghendrih et al., Phys. Fluids B4 (1992) 1287; Plasma Phys. Contr. Fusion 32 (1990) 103; Ph. Ghendrih, Phys. Plasmas 1 (1994) 1929.
[12] G. Telesca, U. Samm et al., Nucl. Fusion 36 (1996) 347.
[13] U. Samm, P. Bogen et al., J. Nucl. Mater. 220–222 (1995) 25.
[14] J.D. Strachan, F.P. Boody et al., Proc. 12th EPS Conf., Budapest, Europhys. Conf. Abstr. (1985) I-339.
[15] J.D. Strachan, F.P. Boody et al., J. Nucl. Mater. 145–147 (1987) 186.
[16] C.E. Bush, J.D. Strachan et al., Neutral Beam Heating of Detached Plasmas in TFTR, Report PPPL-2616 (1989).
[17] G.M. McCracken et al., Proc. 17th EPS Conf., Amsterdam, 1990, Europhys. Conf. Abstr. 14B (1990) III–1381.
[18] U. Samm, G. Bertschinger et al., Proc. 18th EPS Conf., Berlin, 1991, Europhys. Conf. Abstr. 15B (1991) III–157.
[19] J.C. Vallet, L. Poutchy et al., Phys. Rev. Lett. 67 (1991) 2662.
[20] B. Lipschultz, J. Nucl. Mater. 145–147 (1987) 15.
[21] B. Lipschultz, Proc. Satellite Workshop of the 9th PSI Conf., Cadarache, 28–30 May (1990), report EUR-CEA-FC-1403.
[22] C.G. Lowry et al., Proc. 17th EPS Conf., Amsterdam, 1990, Europhys. Conf. Abstr. 14B (1990) I–339.
[23] K. Borrass et al., Nucl. Fusion 33 (1993) 63.
[24] P. Monier-Garbet, C. Chamouard et al., Proc. 21st EPS Conf., Montpellier, 1994, Europhys. Conf. Abstr. 18B (1994) II–738.
[25] G. Janeschitz, R. König et al., J. Nucl. Mater. 196–198 (1992) 380–385.
[26] D.E. Post, J. Nucl. Mater. 220–222 (1995) 143.
[27] U. Samm, P. Bogen et al., J. Nucl. Mater. 176&177 (1990) 273.
[28] M.Z. Tokar, Nucl. Fusion 34 (1994) 853.
[29] M.Z. Tokar, Plasma Phys. Contr. Fusion 36 (1994) 1819.
[30] M.Z. Tokar and H. Lasaar, to be published.
[31] M. Mattioli, C. DeMichelis and P. Monier-Garbet, Nucl. Fusion 35 (1995) 807.
[32] C. DeMichelis, A. Grosman et al., Proc. 22nd EPS Conf.,

Bournemouth, 1995, Europhys. Conf. Abstr. 19C (1995) III–109.
[33] G. Janeschitz, ITER-JCT and Home Teams, Plasma Phys. Control. Fusion 37 (1995) A19.
[34] B. Unterberg, H. Knauf et al., J. Nucl. Mater. 220–222 (1995) 462.
[35] S.J. Tobin, J.T. Hogan et al., Plasma Phys. Control. Fusion 38 (1996) 251.
[36] P. Monier-Garbet, C. DeMichelis et al., 14th IAEA Int. Conf. on Plasma Phys. and Controlled Nucl. Fusion Res., Vol. 1, Würzburg, 1992 (IAEA, Vienna, 1993) p. 317.
[37] Von Hellermann, K. Barth et al., Proc. 22nd EPS Conf., Bournemouth, 1995, Europhys. Conf. Abstr. 19C (1995) II–009.
[38] T. Loarer, M. Chatelier et al., Plasma Phys. Control. Fusion 37 (1995) A203.
[39] J. Ongena, A.M. Messiaen et al., Plasma Phys. Control. Fusion 38 (1996) 279.
[40] J. Neuhauser, M. Alexander et al., Plasma Phys. Control. Fusion 37 (1995) A37.